# Unveiling the Dynamics of Snow Settling in Atmospheric Turbulence: A Review of Nearly a Decade of Field Research at EOLOS, MN

Jiaqi Li[1,2] and Jiarong Hong[1,2(✉)]

[1] Saint Anthony Falls Laboratory, University of Minnesota, Minneapolis, MN 55414, USA
[2] Department of Mechanical Engineering, University of Minnesota, Minneapolis, MN 55455, USA
jhong@umn.edu

**Abstract.** This paper provides a comprehensive synthesis of a decade's advancements in field investigations into snow settling dynamics, carried out at the EOLOS field research station in Rosemount, MN, USA. The research deployed a succession of progressively sophisticated particle characterization and tracking systems, culminating in the development of a 3D particle tracking velocimetry (PTV) system. Our findings show the compelling role of preferential sweeping mechanisms, noting a consistent enhancement in snow particle settling velocities in association with turbulent eddies across multiple deployments. However, the magnitude of this turbulence-induced enhancement displayed variability, potentially modulated by the differences in turbulence and snow conditions inherent to each deployment. Additionally, intriguing patterns in snow clustering were revealed, characterized by an exponent power-law decay of -2 in cluster size distribution. This, coupled with a vertical orientation of clusters indicative of gravitational influences, adds a layer of complexity to our understanding of snow dynamics. Our research further deciphers the interplay between preferential sweeping and the preferential concentration, or clustering, of snow particles. Higher concentrations of snow particles were consistently found on the downward side of vortices, irrespective of vortex type, with an accelerated settling in these regions. Intriguingly, this disparity in average settling velocity was more pronounced in the case of prograde vortices. The advent of 3D particle tracking velocimetry (PTV) has allowed a nuanced examination of 3D settling trajectories and clustering dynamics. By providing insights into the intricate movements of snow particles as they traverse atmospheric turbulence, it uncovers the subtle variations in motion that could be overlooked in a 2D analysis. These findings offer valuable insights into the effects of snow particle morphology and turbulence on settling dynamics, promising to improve the accuracy of snowfall forecasts and ground snow accumulation predictions.


X. Zheng and S. Balachandar (Eds.): IUTAM 2023, IUTAM Bookseries 41, pp. 58–82, 2024.
https://doi.org/10.1007/978-3-031-47258-9_4

**Keywords:** snow settling · snow clustering · PIV · PTV · field measurement

## 1 Introduction

Predicting ground snow accumulation is a pivotal task, touching on diverse applications from anticipating flood risk due to snowmelt [31], providing avalanche hazard warnings [45], to ensuring traffic safety during snowfalls [37]. This prediction hinges heavily on understanding the intricacies of snow settling dynamics in the atmosphere [24], a process that is far from simple. Influenced by the morphological characteristics of snow particles and the impacts of atmospheric turbulence, it presents challenges that are not easily replicated in lab conditions or numerical simulations. Cloud conditions, including temperature and humidity, can dramatically shape the morphology of snow particles [29], thus altering their settling velocities. These velocities can fluctuate from virtually zero to up to 3 m/s [16,28], adding a dynamic element to the snow's path as it descends from cloud to ground, possibly drifting over vast distances. Atmospheric turbulence, known for its complex structures and high Reynolds numbers, introduces an additional layer of complexity to the settling process. This complexity underscores the need for more comprehensive research into the physical mechanisms underlying snow settling, to not only improve the precision of snow accumulation models but also enhance our ability to predict and prepare for the diverse impacts of snowfall.

In the previous scientific investigations, the influence of snow morphology on settling velocity has received much attention, although earlier studies did not explicitly account for the impact of atmospheric turbulence. The pioneering empirical work of Locatelli & Hobbs [28] laid the groundwork by establishing correlations between snow particle dimensions, mass, and settling velocity, each tailored to distinct snow morphologies through field measurements. Passarelli [39] examined the effect of snow collection efficiency on the formation of aggregates and their subsequent fall speed. Moreover, Mitchell, Zhang & Pitter [34] explored the snowfall rate under the influence of riming, a process in which supercooled water droplets deposit on snow crystals. The advent of the Multi-Angle Snowflake Camera (MASC) system [15] marked a significant breakthrough, providing a more nuanced approach to assessing snow morphology and settling velocity across diverse snow types. On the theoretical and modeling front, Böhm [8] proposed a universal model to estimate snow settling velocity, encapsulating the correlation among drag coefficient, particle Reynolds number, and Best number. His model ingeniously linked particle shape and settling dynamics by considering the ratio of the actual snow projected area to the elliptical area enclosing it. Building on Böhm's foundational work, Mitchell & Heymsfield [33] advanced the understanding of ice particle fall speeds across a range of shapes, refining the relationship between Reynolds number and Best number. Heymsfield & Westbrook [20] then introduced new computational methods for predicting snow fall speed. Their approach, grounded in laboratory measurements on various snow

morphologies, effectively corrects the projected area ratio bias. These collective efforts underscore the pivotal role of snow morphology in understanding and predicting snow settling velocity.

Taking the study beyond morphology alone, it becomes apparent that atmospheric turbulence plays a considerable role in snow settling dynamics. The complexity of this influence is evident when considering that snow particles, given their range of shapes, sizes, and densities greater than surrounding air, effectively behave as heavy inertial particles within turbulent conditions. This behavior results in characteristic patterns, such as clustering and settling velocity modulation, strongly indicating the presence of intricate particle-turbulence interactions [6]. Influenced by factors like turbulence characteristics, represented by the Kolmogorov time scale, $\tau_\eta$, and particle properties such as size ($D_p$), density ($\rho_p$), and aerodynamic characteristics. These particle properties collectively define the particle response time, $\tau_p$ [32], a key mechanism within this dynamic unfolds. This mechanism, known as preferential sweeping, leads particles to accumulate in strain-dominated regions, descending as clusters [3,12,17,55,56], and can significantly amplify the settling velocity when the Stokes number $St = \tau_p/\tau_\eta$ is around 1 [3,14,42,56]. However, it is important to highlight that much of the existing literature has been based on the simplified assumption of spherical or point particles, which overlooks the intricate diversity of snow morphologies, suggesting a crucial gap that future research needs to address in order to enhance our understanding of snow settling dynamics in turbulent conditions.

Moving beyond the common assumption of spherical particles in particle-turbulence interaction studies, several investigations have expanded their scope to consider non-spherical geometries, including disks, ellipsoids, and fibers. This shift in focus has yielded valuable insights into the settling behavior of non-spherical particles in turbulence, revealing unique mechanisms influenced by turbulence. Among these mechanisms, the preferential orientation of non-spherical particles has emerged as a significant factor, as has the presence of preferential sweeping [44]. Notably, the work by Siewert et al. [44] employed direct numerical simulation (DNS) to delve into these phenomena, providing a robust computational perspective. Voth & Soldati [54] further contributed to this field with a comprehensive review of anisotropic particles in turbulence, reinforcing the importance of considering non-spherical particles in such studies. A standout study in this area is the work by Esteban, Shrimpton, & Ganapathisubramani [11], who meticulously examined the settling dynamics of disk-shaped particles in turbulence. Using a stereoscopic vision system consisting of two digital cameras and a diffuse light source, they traced the complex three-dimensional trajectories of these particles. Their work revealed an intriguing correlation between the natural frequency of particles and the turbulent flow frequency at the particle length scale. While these investigations have advanced our understanding of non-spherical particles within turbulence, they do not fully encapsulate the realistic scenario of snow settling dynamics due to the inherent simplification in the chosen particle geometries.

Despite substantial efforts in laboratory experiments and simulations, a conspicuous gap persists in field data regarding the settling of inertial particles, such as snow, droplets, and dust, in atmospheric turbulence. This shortage in data is largely attributed to the inherent challenges in performing field measurements [43], including the need to parameterize local turbulent field conditions and the complex task of discerning the influences of particle interaction and flow Reynolds numbers on non-Stokesian particle kinematics. Notable strides in this area have been made recently [12,40,52], yet limitations persist. Incorporating particle-turbulence interaction mechanisms into predictive models at geophysical scales remains particularly challenging due to the disparity in conditions between the field and laboratory or simulation environments. The conventional models that typically utilize simplified ellipsoidal shapes for particles fall short in accurately representing the drag coefficient and wake characteristics of genuine snow particles [46,47].

Addressing the compelling challenges of field measurements, our team has implemented and advanced the snow particle imaging approach, initially applied in the study of wind turbine wake flows [1,10,21] and atmospheric boundary layer research [18,51]. This systematic refinement of these methodologies, spanning nearly a decade, has allowed us to delve into the complex dynamics of snow settling within natural environments, providing invaluable firsthand observations that incorporate both the snow morphology and the influence of turbulence. The present paper is not just a summary of previous publications but represents a distillation of nearly a decade's worth of dedicated effort in field measurements and research into snow settling dynamics. It brings together our key findings encapsulated in four landmark publications [9,25,26,36], each contributing unique insights and advancements to the study of this intricate phenomenon. Moreover, the review process has allowed us to synthesize these contributions and extract new insights. The layout of this paper is thoughtfully structured: Sect. 2 offers a comprehensive overview of our approach, detailing the progression of field experiments and data analysis techniques, specifically centered on the intersection of snow particle dynamics and atmospheric turbulence. Section 3 collates the significant findings from our sustained field campaign, drawing upon the insights from the referenced publications and previewing our ongoing research initiatives. Concluding in Sect. 4, we reflect on the valuable insights and the journey of our dedicated research into the complex process of snow settling. This final section also proposes future research avenues, acknowledges the limitations encountered in this journey, and explores potential strategies to overcome these challenges.

## 2 Methods

Over the span of the last decade, our research team has undertaken more than 15 field deployments at the EOLOS field research station in Rosemount, MN. These deployments have been instrumental in our ongoing exploration of snow settling dynamics. To delve into this complex phenomenon, we have harnessed a range of innovative imaging techniques, including planar particle tracking velocimetry (PTV), simultaneous planar super-large-scale particle image velocimetry

(SLPIV) and PTV, field 3D PTV, and a pioneering snow particle characterization tool that employs digital inline holography (DIH). The utilization of these advanced methodologies has propelled us into uncharted territory in the study of snow settling dynamics.

The EOLOS field station, initially established as a wind energy research facility and equipped with a 2.5 MW turbine and a 130 m meteorological tower, has proven to be a unique site for our snow settling studies. The station's relatively open terrain, with minimal canopy interference, provides an ideal setting for capturing video footage of snow settling under a wide range of conditions. The meteorological tower is fitted with a comprehensive suite of sensors that measure wind velocity, temperature, and humidity, which are essential for characterizing the atmospheric and turbulence conditions during our field experiments. Specifically, the tower hosts four sonic anemometers and temperature sensors (CSAT3, Campbell Scientific), operating at a 20 Hz sampling rate, strategically placed at elevations of 10, 30, 80, and 129 m. Additionally, six cup-and-vane anemometers, along with temperature and humidity sensors (1 Hz sampling rate), are installed at 7, 27, 52, 77, 102, and 126 m elevations. This extensive sensor setup enhances our ability to collect detailed and accurate data.

In this paper, we turn our focus to five major deployments that have been the subject of our previous publications. Each of these deployments was conducted under unique flow and snow conditions, which were analyzed to understand their impact on snow settling dynamics. To quantify the atmospheric and turbulent conditions during each deployment, we utilized the sonic anemometer at 10-m elevation and other sensors installed on the meteorological tower. Key parameters for each deployment, including atmospheric stability, integral time scale, length scale, and turbulence dissipation rate, etc., are summarized in Table 1. The atmospheric stability was estimated using the bulk Richardson number ($R_b$) and the Monin-Obukhov length ($L_{OB}$). The integral time scale ($\tau_L$) and the length scale ($L$) were estimated based on the temporal autocorrelation function of the streamwise velocity. The turbulence dissipation rate ($\epsilon$) was estimated using the second-order structure function of the streamwise velocity component,

**Table 1.** Estimated meteorological and turbulence conditions from the sonic anemometer at $z = 10$ m. See the text for the definition of the symbols. Note that Bristow et al. [9] only provides mean flow conditions for Apr. 2022 deployment not the turbulence statistics.

| Dataset | $U$ (m/s) | $u_{\mathrm{rms}}$ (m/s) | $R_b$ (−) | $L_{OB}$ (m) | $L$ (m) | $\tau_L$ (s) | $\epsilon$ $(\mathrm{cm}^2/\mathrm{s}^3)$ | $\eta$ (mm) | $\tau_\eta$ (ms) | $Re_\lambda$ (−) |
|---|---|---|---|---|---|---|---|---|---|---|
| Jan. 2016 | 1.98 | 0.16 | 0.03 | 811 | 4.9 | 30.6 | 8 | 1.29 | 126 | 938 |
| Nov. 2018 | 1.55 | 0.38 | 0.12 | 1007 | 3.4 | 8.9 | 21 | 1.04 | 83 | 3548 |
| Jan. 2019 | 5.95 | 1.18 | 0.03 | -2643 | 14.6 | 12.9 | 314 | 0.49 | 20 | 9180 |
| Jan. 2020 | 5.47 | 1.07 | 0.16 | 1651 | 6.2 | 5.8 | 355 | 0.51 | 19.4 | 6478 |
| Apr. 2022 | 1.69 | 0.27 | 0.08 | 191 | 1.47 | 5.35 | 9.7 | 1.2 | 117 | 2558 |

with the Taylor hypothesis employed to convert the measured time series into spatial velocity variations. For a more detailed discussion of the methods and equations used in these calculations, we refer readers to our previous publications [25,26,36]. This comprehensive analysis of the atmospheric and turbulent conditions during each deployment has provided us with a deeper understanding of their implications on snow settling dynamics.

Shifting focus from atmospheric and turbulent conditions to the specifics of our snow particle measurements, it is pertinent to note the significant advancements we have achieved using the digital inline holography (DIH) technique for capturing the morphology of snow particles. The evolution of our snow analyzer technology, which has seen two distinct generations of development, is depicted in Fig. 1. Figure 1a illustrates the first-generation snow particle analyzer, a DIH sensor mounted atop a field vehicle, an effective but comparatively rudimentary system. Recognizing the need for more comprehensive data, we developed a second-generation snow particle analyzer that greatly enhanced our measurement capabilities. Shown in Fig. 1b, this new analyzer combines the DIH sensor with a high-precision scale to measure snow particle weight, thereby enabling simultaneous measurement of particle size, shape, type, and density. The improved data accuracy and expanded scope of our second-generation analyzer necessitated a more advanced data processing solution. To meet this need,

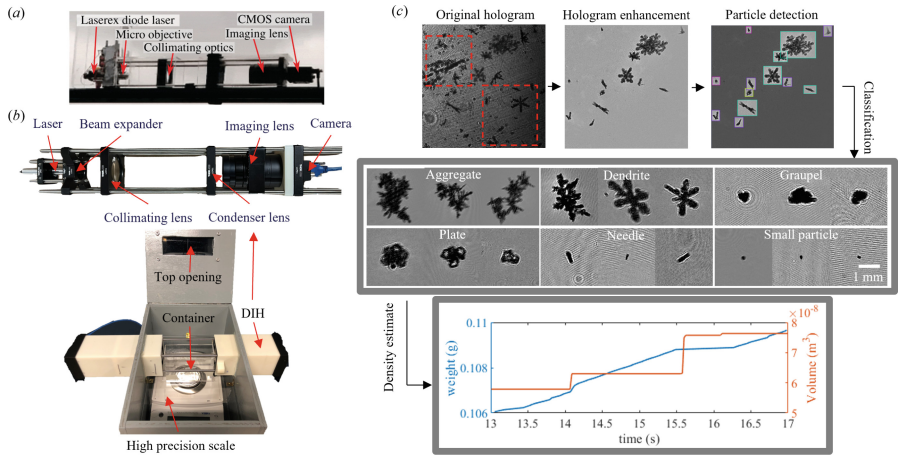


**Fig. 1.** (a) First-generation snow particle analyzer based on digital inline holography (DIH) sensor mounted atop a field vehicle. (b) Second-generation snow particle analyzer designed for simultaneous measurement of particle size, shape, type, and density, combining the DIH sensor and a high precision scale. (c) Real-time data processing software developed for the second-generation snow particle analyzer. The software includes image enhancement to eliminate static background (highlighted in red dashed boxes), snow particle detection and categorization using machine learning models, and particle volume and density estimation derived from weight measurements on a high-precision scale.

we developed real-time data processing software, as demonstrated in Fig. 1c. This custom software, built around the YOLOv5 machine learning model, is capable of image enhancement, snow particle detection, categorization, and estimation of particle volume and density derived from weight measurements on the high-precision scale. The software categorizes snow particles into six types according to their shape and aerodynamic response, achieving an impressive 99% particle detection rate and an average classification accuracy of 95%. For a more comprehensive understanding of the snow particle analyzer's development and operation, readers are referred to [27].

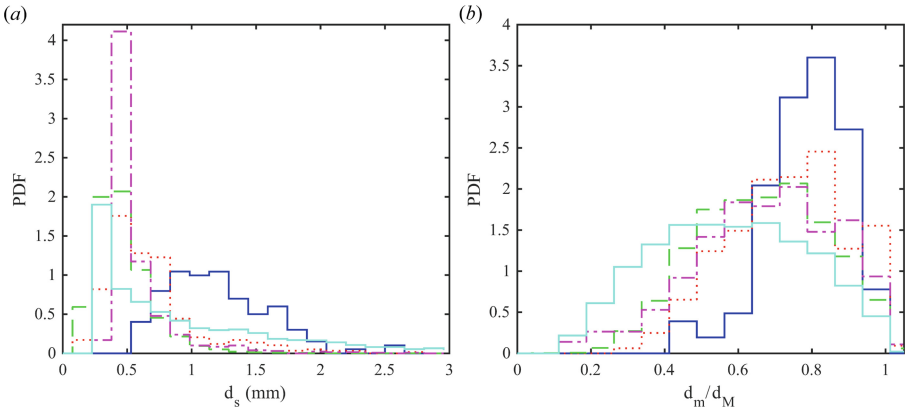


**Fig. 2.** The probability density functions (PDFs) of (a) size ($d_s$) and (b) aspect ratio ($d_m/d_M$) of the snow particles for January 2016 (solid blue line), November 2018 (dotted red line), January 2019 (dashed green line), January 2020 (dash-dotted magenta line), and April 2022 (solid cyan line).

With the particulars of our snow particle measurement technique established, we then focus on the resulting data. The probability distribution functions (PDFs) of snow particle size and aspect ratio are presented in Fig. 2. This figure provides a comparative analysis of data from the five deployments, offering insights into the variations in snow particle characteristics under different conditions. Complementing the graphical data in Fig. 2, Table 2 consolidates the mean values, standard deviations of particle diameter and aspect ratio, and estimates of snow number concentration and volume fraction from the different deployments.

With the advancement of our measurement techniques in quantifying turbulence and snow particle conditions, we concurrently developed a method based on light sheet-based particle tracking velocimetry (PTV). This technique, which proved vital in tracing the snow settling trajectory and concentration distribution of snow particles, was rooted in the super-large-scale particle image velocimetry (SLPIV) methods established by [21,51]. The experimental setup for this method is illustrated in Fig. 3a. In Fig. 3a, the setup integrates a 5-kW

**Table 2.** The snow particle properties and concentration measured using the snow analyzers from different deployments.

| Dataset | Mean diameter $d$ ( mm) | Aspect ratio $d_{\mathrm{maj}}/d_{\mathrm{min}}$ $(-)$ | Number concentration $N$ $\left(\mathrm{m}^{-3}\right)$ | Volume fraction $\phi_V \times 10^{-7}$ $(-)$ |
|---|---|---|---|---|
| Jan. 2016 | $1.09 \pm 0.45$ | $0.73 \pm 0.11$ | 816 | 7.4 |
| Nov. 2018 | $0.65 \pm 0.41$ | $0.65 \pm 0.16$ | 1644 | 6.3 |
| Jan. 2019 | $0.39 \pm 0.23$ | $0.57 \pm 0.17$ | 56620 | 44 |
| Jan. 2020 | $0.39 \pm 0.29$ | $0.62 \pm 0.15$ | 28460 | 38 |
| Apr. 2022 | $0.97 \pm 0.90$ | $0.54 \pm 0.21$ | 933 | 17 |

searchlight paired with a curved mirror to vertically expand the beam into a light sheet. This light sheet illuminates the snow particles, and it is oriented parallel to the average wind direction to minimize out-of-plane motion. Typically, this setup is positioned 50 m upwind or downwind of the meteorological tower, thus enhancing the precision of the flow condition quantification. Along with the illumination setup, our measurement approach employs a Sony A7RII (Sony Corp.) camera to capture detailed particle motion. This camera records at a high frame rate of 120 FPS and a resolution of 720 × 1280 pixels within a targeted field of view. Table 3 details the field of view and other specifications pertinent to this camera.

To enable the elucidation of the underlying mechanism of the flow-particle interaction, we implemented a dual-camera setup, as shown in Fig. 3b. This setup complements the Sony camera with a Nikon D600 (Nikon Inc.) camera, thereby enabling simultaneous measurements of the turbulent flow field and snow particle trajectories. The Nikon camera is configured to record a broader field of view at a frame rate of 30 FPS and a resolution of 1080 × 1920 pixels, providing a comprehensive view of the overall turbulent flow field. Both cameras, referred to as PTV (Sony A7RII) and SLPIV (Nikon D600) in the subsequent sections, are mounted on tripods, with their specifications documented in Table 3.

To process the data captured through our PTV and simultaneous SLPIV/PTV systems, we utilized particle image velocimetry (PIV) analysis with the aid of LaVision Davis 8.2.0 software. We employed a multi-pass setting, with the final pass configured to 32 × 32 pixels and a 50% overlap, ensuring a comprehensive analysis of the captured data. For the extraction of particle Lagrangian trajectories, we turned to the four-frame best estimate algorithm, a method proposed by Ouellette, Xu & Bodenschatz [38]. This algorithm proved to be a solid foundation for our data extraction process. Building on this foundation, we implemented the learning-based method developed by Mallery, Shao & Hong [30] in our most recent study. This method further enhanced our ability to accurately track and analyze the trajectories of snow particles.

In our latest research endeavor, we have designed and implemented a mobile field 3D PTV system, as detailed in [9]. This system, illustrated in Fig. 3c, is

engineered to capture the intricate 3D settling dynamics of snow particles. The system consists of four Wi-Fi synchronized cameras, arranged in a fan-like array spanning 90°C. These cameras surround a light cone, which is reflected and expanded by a curved mirror from the same searchlight used in our planar measurements. Each camera is positioned 5.5 m away from the searchlight and angled at 58°C, looking upward at a height of 10 m above the ground. Moreover, each camera is outfitted with an enclosed data acquisition unit, housing a board-level computer for image capturing commands, a solid-state drive for system and image storage, and a power supply. To ensure accurate measurements, we employ a calibration process using an unmanned drone equipped with two colored LEDs, set 34.5 cm apart on a wand. This calibration process is based on the wand calibration method [49]. We have developed a custom-designed camera control software that synchronizes the image capturing process across all four

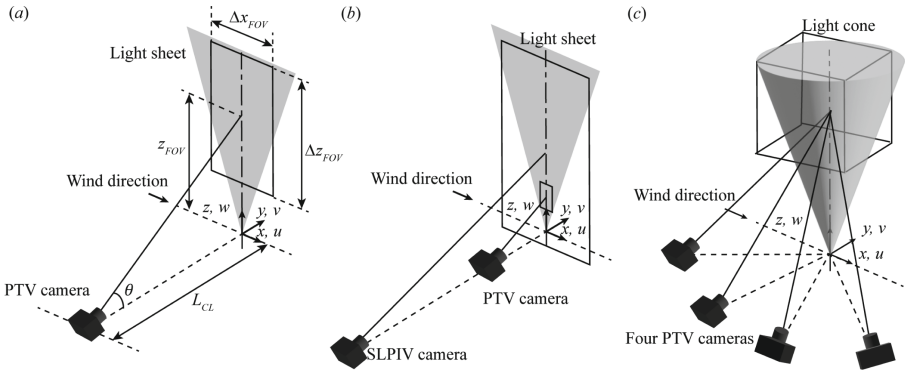


**Fig. 3.** Illustrations of the experimental setups used for field snow settling measurements, including (a) the planar particle tracking velocimetry (PTV) measurement setup, (b) the setup enabling simultaneous measurements using super-large-scale particle image velocimetry (SLPIV) and PTV, and (c) the ground-based multiview field 3D PTV measurement setup.

**Table 3.** Summary of key parameters of the super-large-scale particle image velocimetry (SLPIV), particle tracking velocimetry (PTV), and 3D field PTV measurement set-ups for the deployment dataset used in the present paper. Here FOV denotes field of view.

| Dataset | SLPIV/PTV setup | | | | | | DIH setup | |
|---|---|---|---|---|---|---|---|---|
| | Duration (min) | $z_{FOV}$ ( m) | $\Delta x_{FOV} \times \Delta z_{FOV}$ ( $m^2$) | Resolution (mm/ pixel ) | $\theta$ ( deg. ) | $L_{CL}$ ( m) | Resolution ($\mu$m/ pixel ) | Volume ($cm^3$) |
| Jan. 2016 | 5 | 10.8 | $7.1 \times 4.0$ | 5.6 | 21.1 | 25 | 24 | 18.8 |
| Nov. 2018 | 17 | 9.1 | $8.4 \times 4.7$ | 6.5 | 14.5 | 31 | 14 | 42 |
| Jan. 2019 | 15 | 20.2 | $14.7 \times 8.3$ | 12.0 | 19.9 | 53 | 14 | 42 |
| Jan. 2020 | 11 | 18.4 | $39.2 \times 22.1$ | 20.5 | 19.9 | 53 | 14 | 42 |
| | 11 | 7.9 | $5.3 \times 3.0$ | 4.2 | 18.4 | 19.1 | | |
| Apr. 2022 | 1 | 10 | $4 \times 4\,(\Delta y_{FOV}) \times 6$ | 6.3 | 58 | 5.5 | 14 | 88 |

cameras. Once calibrated, the snow particle trajectories are obtained using an open-source implementation of the shake-the-box (STB) method [48]. The measurement sample volume of this setup is 4 m × 4 m × 6 m, offering a resolution of 6.3 mm per voxel, as summarized in Table 3.

## 3 Results

In this section, we aim to provide a succinct review of our recent advancements in the 2D field measurement of snow settling dynamics, while also offering a preview of our ongoing work on 3D PTV field measurements. The primary focus will be on the outcomes of our measurements, the comparisons drawn between different deployments, and the novel physical insights and implications that have emerged from these observations. A key aspect of this review will be the new insights gained from cross-comparison of different deployments, which go beyond the findings reported in the original papers. For a more detailed understanding of the techniques and data analysis tools that form the foundation of these findings, we recommend referring to our recent publications [9,25,26,36].

### 3.1 Preferential Enhancement of Snow Particle Settling

In this section, we explore the impact of turbulence on the settling velocity of snow particles, a pivotal aspect of our study. This exploration is grounded in data from several deployments, including those documented in [25,36], and [26]. Our primary objective is to compare the terminal velocity of snow particles in still air with their measured settling velocity under the influence of atmospheric turbulence.

To estimate the terminal velocity of snow particles, we first need to determine their aerodynamic response time, which is extrapolated from the probability density functions (PDFs) of normalized snow particle acceleration ($a_p/\langle a_p^2 \rangle^{1/2}$). As depicted in Fig. 4a, the blue triangles correspond to data from January 2016 [36], the red diamonds to November 2018 [25], and the magenta squares to January 2020 [26]. Our findings are compared with previous experimental and simulation measurements [5,7,35]. The acceleration PDFs of January 2016 and November 2018 are well-defined, facilitating the estimation of the range of Stokes numbers ($St$). However, the PDF for January 2020 shows larger variability, with the probability density approaching that of November 2018 in the lower range of normalized accelerations but approaching that of January 2016 for higher values. It is important to note that while the kurtosis of the acceleration PDFs is sensitive to the Stokes number of the particles, the influence of turbulence properties, particularly the Taylor microscale Reynolds number ($Re_\lambda$), on the acceleration distribution of snow particles remains an active area of research. Existing simulations and experimental findings [22,23,53] suggest an increase in acceleration kurtosis for both fluid tracers and inertial particles with $Re_\lambda$. However, the effect of $Re_\lambda$ on acceleration kurtosis might be relatively minor in the high Reynolds number regime [22]. Given these considerations, we have

estimated the Stokes numbers for the snow particles based on three separate particle tracking velocimetry (PTV) deployment datasets. The estimated ranges of Stokes numbers are as follows: 0.09–0.37 for January 2016, 0.15–1.01 for November 2018, and 0.09–1.01 for January 2020. These ranges reflect the variability in the Stokes numbers of snow particles, influenced by factors such as size, shape, and density.

Building on the estimated range of Stokes numbers, we can leverage the Kolmogorov time scale of turbulence ($\tau_\eta$) to calculate the particle aerodynamic response time ($\tau_p = St \cdot \tau_\eta = W_t/g$). This calculation allows us to also predict the terminal velocity of snow particles in still air ($W_t$). The estimated terminal velocity ranges are as follows: 0.12–0.47 m/s for January 2016, 0.12–0.82 m/s for November 2018, and 0.02–0.19 m/s for January 2020. The notably smaller terminal velocity for January 2020 can be attributed to the smallest particle size and the significantly smaller turbulence Kolmogorov time scale used for its estimation. In Fig. 4b, we compare the predicted terminal velocity ($W_t$) of snow particles with the settling velocity ($w_p$) as measured through PTV in the field. Across all three deployments, we observed an increase in settling velocity under the influence of turbulence. However, the most substantial enhancement was recorded in the January 2020 deployment. Specifically, the average settling velocity observed during the January 2020 deployment was seven times greater than the predicted terminal velocity, which was significantly higher than those derived from the January 2016 and November 2018 datasets. This pronounced enhancement in settling velocity during the January 2020 deployment may be largely attributed to the more intense turbulence conditions during this period,

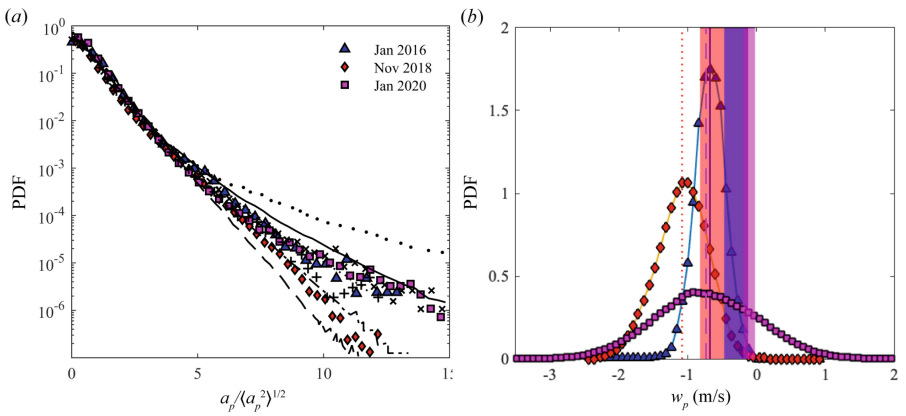


**Fig. 4.** (a) Probability density functions (PDFs) of normalized in-plane snow particle acceleration from different PTV deployments, compared with St = 0 from [35] (dots), [7] (St = 0.16, solid line; St = 0.37, dotted line; St = 1.01, dash-dotted line; St = 2.03, dashed line), and [5] (St = 0.09, ×; St = 0.15, +); (b) comparison of the measured distribution (same symbols as the acceleration PDF) and average (vertical lines, January 2016, blue solid line; November 2018, red dotted line; January 2020, magenta dotted line) of settling velocity with the estimated range of still-air terminal velocities (January 2016, blue region; November 2018, red region; January 2020, magenta region).

as evidenced by the highest Reynolds number ($Re_\lambda$) and dissipation rate among all the datasets. This turbulence condition brought the Stokes number closer to the critical value of '1'. This near-critical Stokes number suggests an optimal dynamic interaction between the snow particles and the turbulent air motion, leading to a heightened settling velocity. Secondarily, the January 2020 deployment had a notably higher snow particle concentration. This increased concentration intensified particle-particle interactions, which could potentially further boost the settling velocity. Though our study offers notable contributions, the conclusions are somewhat influenced by uncertainties due to simplifications in our methodology. Notably, the representation of snow particles as perfect spheres and their assumed size being smaller than the Kolmogorov scale can contribute significantly to the variance in our findings.

### 3.2 Snow Particle Clustering

In this section, we turn our attention to the intriguing phenomenon of snow particle clustering under intense turbulence. This occurrence, often associated with preferential concentration due to turbulence, has substantial implications for regional ground accumulation rates and interactions between particles. The data utilized for this analysis stems from multiple field deployments, as detailed in [25,26].

To delve into this investigation, we need to estimate the concentration of snow particles. This is achieved by analyzing the intensity of images captured through super-large-scale particle image velocimetry (SLPIV), as demonstrated in Fig. 5. As established by [41], there is a linear correlation between the scattered light intensity in PIV images and the number concentration of particles. Consequently, we can compute the estimated relative concentration, denoted as $C^*$, using the formula $C^* = I/\overline{I_{1\ \mathrm{min}}}$. Here, $I$ represents the instantaneous image intensity, while $\overline{I_{1\ \mathrm{min}}}$ denotes the 1-minute moving average of the image intensity. Figure 5 reveals the presence of clustering during both the January 2019 and January 2020 deployments. However, a closer look reveals distinct qualitative differences between the two. The January 2020 sample exhibits larger variability in relative concentration and larger clusters. In contrast, the January 2019 sample displays clusters that resemble thin filaments, extending in the vertical direction.

Expanding upon the initial observations noted in Fig. 5, we pursued a more intricate understanding of snow particle clustering through a thorough quantitative analysis. Figure 6 offers a meticulous comparison of the statistical characteristics tied to cluster morphology across different deployments, thereby highlighting salient variations. Figure 6a focuses on the cluster area ($A_C$) distributions normalized by the Kolmogorov scale ($\eta$), from each deployment. Interestingly, these distributions reveal a power-law decay, echoing patterns seen in prior laboratory assessments and simulations. This decay indicates a self-similarity across clusters of diverse sizes, hinting at the prominent role turbulent eddies play in their formation. An observation of larger clusters in the January 2020 dataset seems to underscore the enhanced influence of turbulence on snow particle concentration and the broader imaging field of view (FOV). Conversely, Fig. 6b

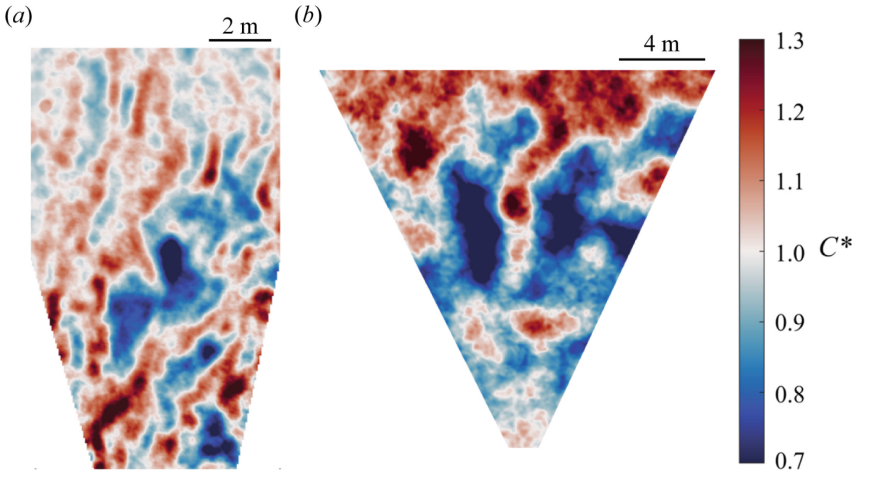


**Fig. 5.** Samples of instantaneous normalized snow concentration map derived from (a) January 2019 and (b) January 2020 deployments.

shifts focus towards the statistical distribution of the aspect ratio ($s_2/s_1$) of the clusters. The elongated shape of clusters in both datasets, most exhibiting an aspect ratio around 0.5, reflects the gravitational forces acting on them. The elongation is not a random trait but a specific characteristic of heavy inertial particles navigating turbulent flows under gravitational pull. Figure 6c offers insight into the orientation ($\theta_C$) of the snow particle clusters, which predominantly assumes a vertical disposition-another testament to gravity's influence. Nevertheless, a notable shift in peak aspect ratio towards one and a more evenly distributed orientation are observed in the clusters from January 2020. This subtle shift indicates a reduced gravitational influence relative to turbulence when compared to the January 2019 data.

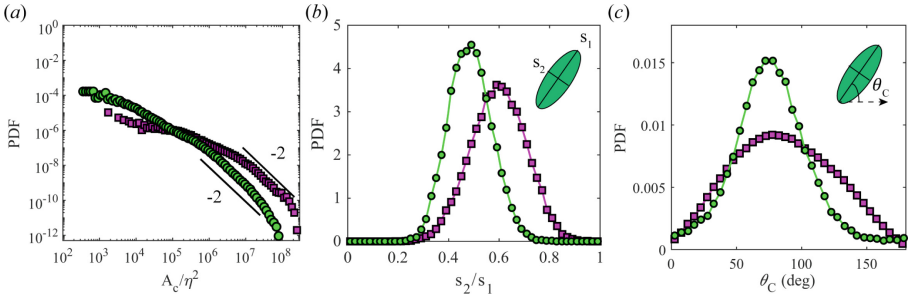


**Fig. 6.** (a) The probability density functions (PDFs) of snow particle cluster area ($A_C$) normalized by Kolmogorov length scale ($\eta$) show a power-law decay with an exponent close to $-2$. The PDFs of (b) the cluster aspect ratio and (c) angle orientation of the clusters. The green circles represent January 2019, and the magenta squares represent January 2020.

Overall, our analysis indicates that the consistent patterns of cluster size and morphology across the datasets signal the presence of universal physical mechanisms **(i.e., the interplay of turbulent eddies and gravitational forces in snow cluster formation)** that dictate clustering behavior. This discovery raises the possibility of constructing predictive models based on these principles. Despite these consistencies, variances across the datasets could be ascribed to the intricate interplay between atmospheric turbulence, gravity, and the unique properties of snow particles. However, considering the similar characteristics of snow particles and turbulence across the datasets, it is plausible that the prominent factor driving the difference in cluster behavior is the elevation variation between sampling zones. Specifically, the January 2020 dataset, for instance, focuses on a lower elevation and hence may capture images within the internal shear layer that is densely populated by potent prograde vortices. These vigorous coherent structures within turbulence could locally overshadow gravity's effects, diminishing cluster elongation and preferential orientation.

### 3.3 Connection Between Preferential Sweeping and Snow Clustering

In this section, we delve deeper into the mechanisms of the enhanced snow particle settling velocity and clustering, focusing on the preferential concentration and preferential sweeping hypothesis. To substantiate these hypotheses, we present direct measurements of the turbulent flow field and snow particle settling trajectories. These measurements, derived from the super-large-scale particle image velocimetry (SLPIV) and particle tracking velocimetry (PTV) deployment presented in [26] and the method section of the current paper, shed light on the intricate interplay between the turbulent coherent structures, snow particle concentration, and settling velocity. The results of these measurements are illustrated in Fig. 7, providing an overview of the turbulent flow field and snow particle settling behavior. Figure 7a presents the swirling strength contour of a sample instantaneous flow field with the mean velocity removed. **The swirling strength, $\lambda_{ci}$, refers to the imaginary part of the complex eigenvalues of the velocity gradient tensor, $\boldsymbol{D} = \nabla \boldsymbol{u}$, and vortices can be identified by a finite $\lambda_{ci}$ value, as explained in** [2]**.** This visualization allows for the identification of turbulence vortices, highlighting both prograde and retrograde vortices based on their direction of rotation. Building on this, Fig. 7b superimposes a snow particle concentration color map, derived from image intensity, onto the identified vortices. This overlay reveals an interesting pattern: enhanced particle concentration on the downward moving side of vortices, suggesting a preferential concentration effect. To further explore the preferential sweeping mechanism, we combine SLPIV and PTV results to track the motion of snow particles around identified vortices. Figure 7c and d illustrate this process for a retrograde vortex and a prograde vortex, respectively. The trajectories of snow particles colored based on the dimensionless time $t^*$, show a clear acceleration in alignment with the downward fluid motion around both types of vortices. Conversely, on the upward moving side of these vortices, falling snow particles

decelerate, even exhibiting a degree of upward motion. This direct observation provides compelling evidence for the preferential sweeping mechanism and its role in enhancing snow particle settling velocity and promoting snow clustering in turbulent flows.

We further reinforce our qualitative observations with statistical evidence, as depicted in Fig. 8. Figure 8a–c display comparative data between ensemble-averaged concentrations sourced from the SLPIV dataset within the core region of vortices and their surroundings, segmented by azimuthal locations for both prograde and retrograde vortices. A conspicuous pattern arises: higher concentrations are found on the downward side of both vortex types, suggesting a mechanism of preferential concentration. Notably, the highest localized concentration is found at the base of the downward side of retrograde vortices, contrasting with the more uniformly high concentration seen in prograde vortices. This disparity might be understood in light of the dominant presence of prograde vortices in internal shear layers, as supported by [18,57]. Their interaction with neighboring

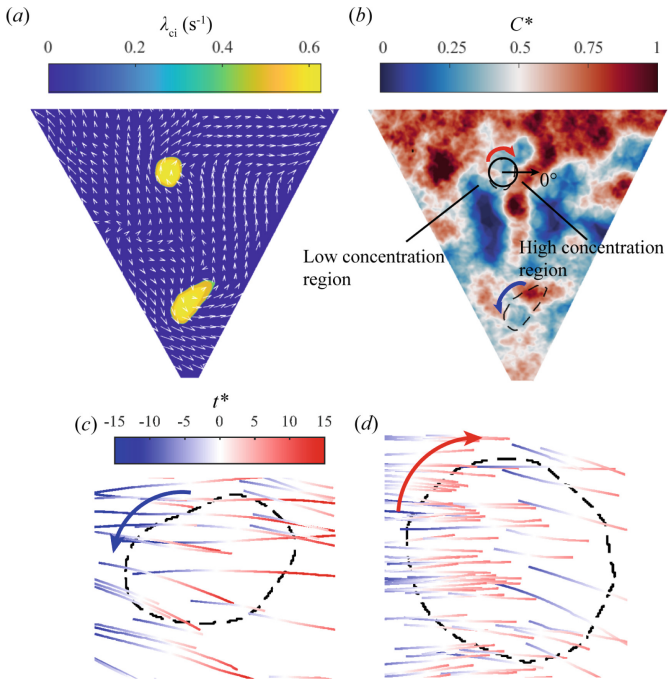


**Fig. 7.** (a) Swirling strength ($\lambda_{ci}$) contour of a sample of instantaneous flow field (mean velocity removed). (b) Corresponding snow particle concentration colourmap ($C^*$ is the relative concentration) with vortices detected from (a). Samples of snow particle trajectories around (c) a retrograde vortex and (d) a prograde vortex. Black dashed lines represent vortex boundaries, and trajectories are colored based on the dimensionless time $t^*$, defined as the difference between the timestamps of snow particles and that of a selected vortex at one time instant normalized by the Kolmogorov time scale. Note that the figure is adapted from [26] with different samples.

vortices likely distributes particle concentration evenly along the downward side. In contrast, the relative isolation of retrograde vortices possibly fosters accumulation of snow particles at their base, likely driven by gravity and descending fluid motion. These findings constitute direct evidence of preferential concentration of snow particles in turbulent eddies, thus marking a significant stride in understanding snow particle dynamics in atmospheric turbulence. Figure 8d and e further deepen our insights by presenting the disparities in the average settling velocities of snow particles on downward and upward sides of both prograde and retrograde vortices, normalized by the average snow settling velocity. In both scenarios, it is apparent that the snow particles settle more swiftly on the downward side of the vortices. A larger disparity in average settling velocity between the downward and upward sides is seen in the case of prograde vortices compared to retrograde ones. This difference may be ascribed to the distinctive self-organization of these vortex types. Specifically, prograde vortices, typically observed in internal shear layers, may yield a compounded effect on enhancing the settling velocity of snow particles.

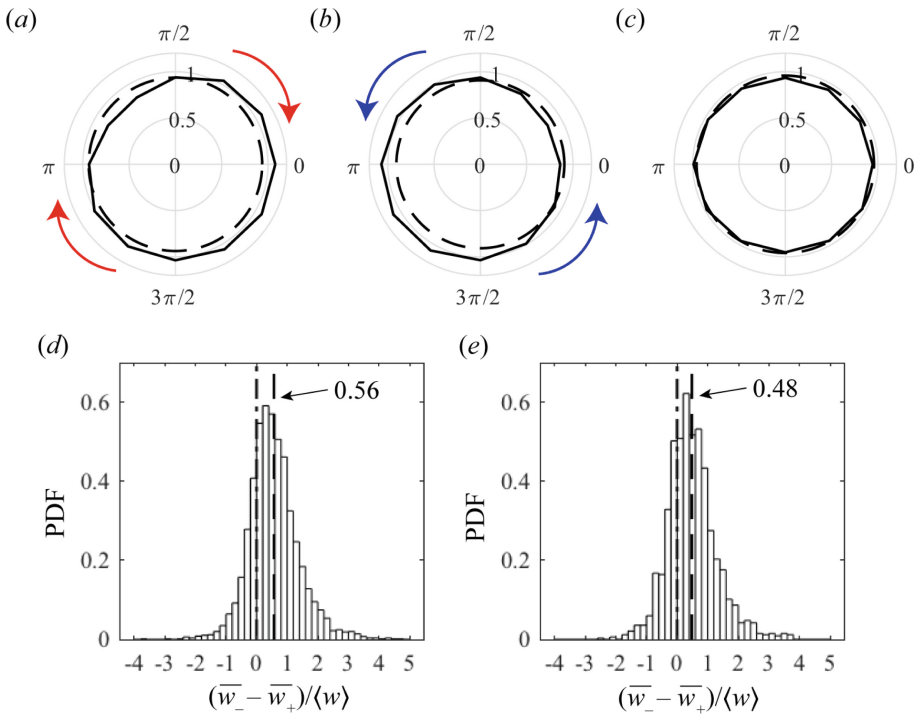


**Fig. 8.** Comparison between the ensemble-averaged concentration from the SLPIV dataset in the central region (dashed lines) of the vortices, and in the proximity (solid lines) for (a) prograde vortices, (b) retrograde vortices and (c) reference background. Histograms of the differences (normalized by the average snow settling velocity $\langle w \rangle$) between the settling velocities on the downward ($\overline{w_-}$) and upward ($\overline{w_+}$) sides for (d) prograde and (e) retrograde vortices.

In summary, this study presents a pioneering direct visualization and quantification of the preferential sweeping of snow particles in atmospheric turbulence. The findings underscore the significant role turbulent vortices play in shaping the interactions between snow particles and atmospheric turbulence while shedding light on the influence these vortices exert on the enhanced settling velocity of snow particles. Additionally, our analysis suggests potential intra-cluster particle interactions. Preferential sweeping might lead to increased particle collision rates within clusters, possibly causing the fragmentation or aggregation of particles. This dynamic interplay has the potential to markedly alter the physical properties of snow particles, thereby influencing their behavior within the turbulent atmospheric environment.

### 3.4 Snow Settling Dynamics in Three Dimensions

While planar measurements have provided significant insights into snow particle dynamics, their two-dimensional nature inherently limits our ability to fully capture the spanwise motion and three-dimensional spatial distribution of snow particles. To overcome these limitations, we have advanced our research methodologies. We have developed a novel three-dimensional (3D) field particle tracking velocimetry (PTV) system, as detailed in a recent publication by [9]. This system enhances our ability to track and analyze the motion of snow particles in a three-dimensional space. In parallel, we have incorporated a snow particle analyzer into our research toolkit, as described in [27]. This tool provides a deeper understanding of the properties of snow particles, including their size, shape, type, and density. By combining these innovative approaches, we can simultaneously monitor various properties of freshly falling snow and track particle settling trajectories in a field setting. This integrated approach not only addresses the limitations of previous methodologies but also paves the way for a more comprehensive understanding of snow particle dynamics.

Capitalizing on advancements in our research methodologies, we executed nine 3D PTV field experiments across the winter seasons of 2021/2022 and 2022/2023. These experiments utilized our novel systems and encompassed a broad spectrum of turbulence and snow conditions. The mean flow ranged from 0.5 to 8.5 m/s, and our observations captured all six prevalent snow particle types: aggregates, dendrites, graupel, plates, needles, and smaller particles. These field experiments inform our ongoing and future endeavors, primarily concentrated on the three-dimensional settling of snow particles. We are particularly keen on dissecting the role of snow morphology and the various turbulence conditions in this process. The preliminary insights gained from these deployments are gradually illuminating the complex behavior of inertial particles within atmospheric flows. A selection of these findings, specifically derived from the dataset of our April 2022 deployment, will be discussed in the section below.

By harnessing our 3D measurement capabilities, we successfully determined the 3D trajectories and corresponding kinematics of snow particles, illustrated in Fig. 9. Figure 9a showcases a selection of snow trajectories, each color-coded

based on its settling velocity. This visual display offers a glimpse into the spatial variability of settling velocities among different particles. Figure 9b further highlights the spanwise acceleration of these particles along their extended trajectories. The periodic variation in spanwise acceleration suggests a meandering motion that may be linked to the dominant presence of dendrite particles in the sample. The particles also display a characteristic trait of inertial particles in turbulence - exponential tails in the acceleration PDFs, depicted in Fig. 9c. A clear asymmetry is noted in the streamwise and vertical acceleration components, which may be attributed to atmospheric flow in the positive $x$ direction and the gravitational force acting on snow particles in the negative $z$ direction. Additionally, our 3D measurements facilitate the extraction of compelling set-

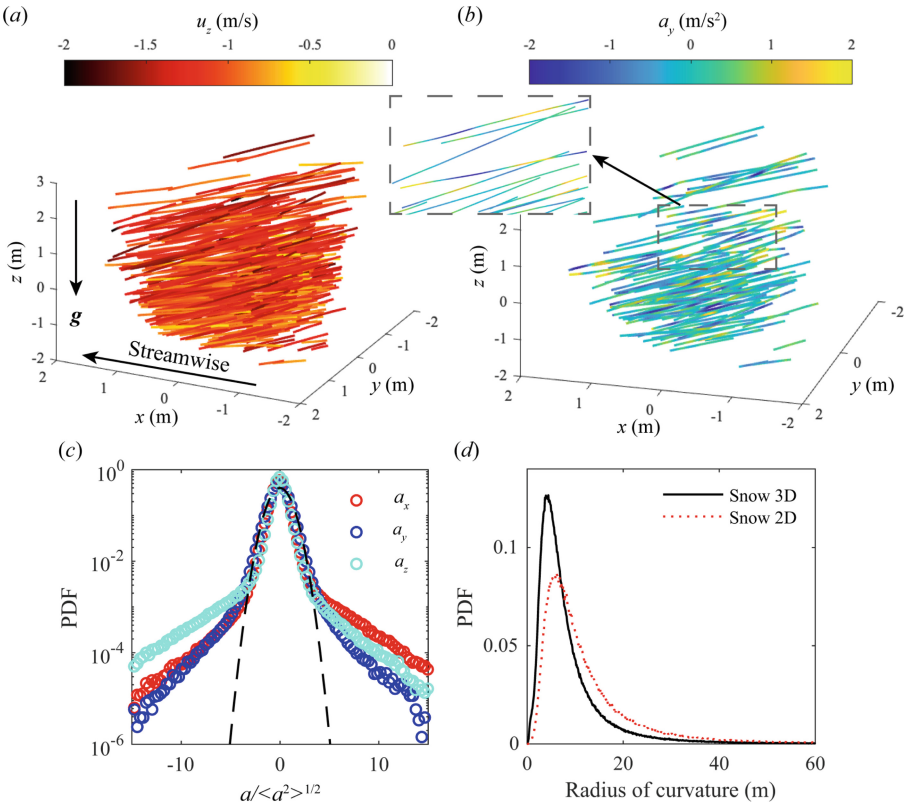


**Fig. 9.** (a, b) Sample snow particle trajectories, colored by (a) vertical velocity, $u_z$, and (b) spanwise acceleration, $a_y$, with the arrows indicating the directions of mean flow (streamwise) and gravity. Probability density functions (PDFs) of (c) acceleration components compared to the corresponding Gaussian distribution (black dashed line), and (d) radii of curvature, where Snow 3D and 2D represent curvature measured using $x$, $y$, $z$ components and $x$, $z$ components, respectively. The results are derived from different dataset from the same deployment as in [9].

tling kinematics, including the curvature of the trajectories. The curvature can be determined using the formula $\kappa = \frac{1}{R} = \frac{\|\boldsymbol{v}\times\boldsymbol{a}\|}{\|\boldsymbol{v}\|^3}$, with R representing the radius of curvature, and $\boldsymbol{v}$ and $\boldsymbol{a}$ denoting the Lagrangian velocity and acceleration, respectively. The $L^2$ norm is symbolized by $\|\cdot\|$. Figure 9d compares the PDFs of the particle trajectory curvature calculated from both full 3D and 2D $x-z$ components. The discrepancies between these distributions underscore the variable spanwise motion, also reflected in Fig. 9b.

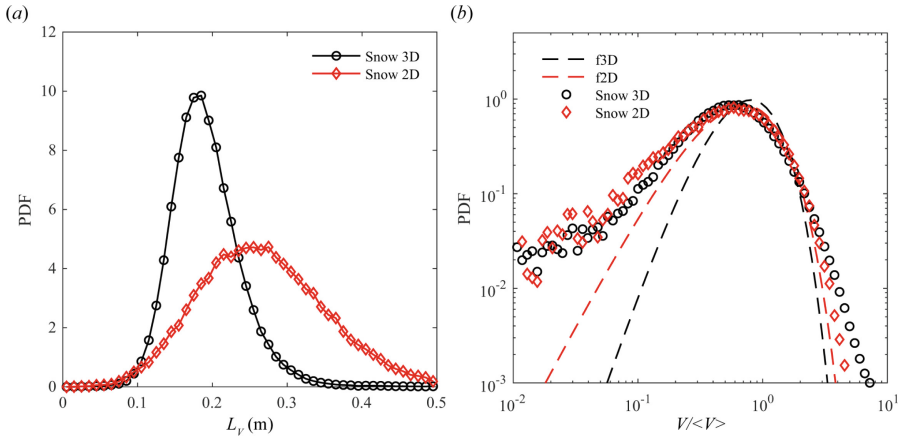


**Fig. 10.** Probability density functions (PDFs) of (a) Voronoi cell length scale $L_V$ and (b) normalized cell volumes $V/\langle V\rangle$, derived from a full 3D volume (snow 3D) and the volume corresponding to a thin slice parallel to the x-z plane extracted from the entire volume (snow 2D). In (b), the results are compared against models f3D and f2D from [13] for randomly distributed particles.

In addition to our Lagrangian analysis, we have incorporated Voronoi analysis, a powerful spatial tessellation technique, to the reconstructed 3D particle field. This method offers a unique perspective on local particle concentration, as it inversely correlates with the volume of each individual tessellation cell. As illustrated in Fig. 10a, the PDFs of the length scales of both 3D and 2D Voronoi cells reveal the typical particle spacing, as indicated by the peak location. The contrast between the 3D and 2D measurements underscores the potential biases introduced by the thin light sheet used in planar measurements, thereby highlighting the value of comprehensive 3D measurements. Delving deeper into our findings, the PDFs of normalized cell volume, as depicted in Fig. 10b, show a higher probability for both small and large cell sizes compared to a random particle distribution. This pattern suggests a clustering tendency among the snow particles. The increased probabilities at both ends of the size spectrum correspond to the snow clusters and voids, respectively. Setting a size threshold for the Voronoi cells allows us to quantify these 3D snow particle clusters, which opens up new avenues for in-depth analysis. For instance, we can delve into a

comparative study of particle settling dynamics within the clusters versus in the voids. This comparison could reveal significant insights into the enhancement or hindrance of settling velocity within these distinct environments. Moreover, we can explore the differences in acceleration dynamics attributable to particle-particle and particle-turbulence interactions. Comprehending these interactions offers potential illumination on the dynamics governing the observed snow particle trajectory behaviors within atmospheric turbulence, while also providing critical insights into the effects of local particle concentration on particle settling and interactions. These prospective analyses underline the remarkable potential of our 3D field imaging approach in propelling forward our knowledge of snow particle behaviors within atmospheric turbulence.

## 4 Conclusions and Discussion

This paper embarked on a comprehensive review, spanning nearly a decade, of field research conducted at the EOLOS Field Research Station, Rosemount, MN, USA, on the subject of snow settling. Utilizing a remarkable array of field imaging tools, we revisited and integrated the outcomes from four previous studies [9,25,26,36]. This undertaking not only served as a capstone for these works, but also spurred the generation of new insights. Our exploration of this research field was made possible through the employment and continuous refinement of a suite of measurement tools, specifically designed for characterizing snow settling dynamics. The technology deployed has evolved through three generations: planar particle tracking velocimetry (PTV), simultaneous super-large-scale particle image velocimetry (SLPIV) and PTV, and field 3D PTV. This endeavor was complemented by the development of a digital inline holography (DIH) method, custom-designed for discerning snow particle types, concentration, and size distribution.

By harnessing the power of these pioneering tools, our work uncovered several intriguing findings. Firstly, data gleaned from multiple deployments consistently point towards the preferential sweeping mechanism. Both statistical evidence and direct imaging unambiguously indicated an enhanced snow settling velocity in conjunction with turbulent eddies. The magnitude of this turbulence-induced enhancement, however, varies across different deployments, likely modulated by diverse turbulence and snow conditions. Secondly, snow clustering-a phenomena observed across different deployments-revealed intriguing trends in cluster size characteristics. An exponent power-law decay of -2 was observed in cluster size distribution across both deployments, while aspect ratio and preferential vertical orientation of clusters suggested gravitational influences. However, detailed distributions, such as mean and standard deviation, seem to be sculpted by the interplay between the significance of turbulent structures, gravity, and snow properties. Thirdly, our direct imaging painted a compelling picture of the interconnection between preferential sweeping and preferential concentration, or clustering, of snow particles. We found that higher concentrations tend to congregate on the downward side of vortices, regardless of rotation direction, and

that snow particles descend more swiftly in these regions. Notably, this disparity in average settling velocity is more pronounced in the case of prograde vortices as compared to their retrograde counterparts. Finally, the deployment of 3D PTV unveiled the intricacies of 3D settling trajectories and the dynamics of snow particle clusters. It offered unprecedented insight into the complex movements of snow particles as they travel through atmospheric turbulence, unveiling subtle variations in motion that might otherwise have been obscured in a 2D analysis.

In general, the research undertaken in this study has led to a variety of valuable insights and findings regarding the interplay of turbulence and snow morphology in the process of snow settling under field conditions. Our work provides extensive field evidence and detailed characterization of the preferential sweep and concentration mechanisms that are essential for understanding snow settling dynamics. By employing novel imaging tools with field research, we have uncovered complex behavioral patterns and identified key contributing factors. However, it is crucial to acknowledge the limitations and challenges encountered in our investigation. One of the most prominent challenges we faced lies in the complexity of disentangling the influence of snow morphology from turbulence on the snow settling dynamics. More specifically, quantifying the exact influence of snow morphology on the aerodynamic response time and settling behavior of snow particles remains a significant hurdle. Our current response time estimations are based on assumptions about snow properties, which, in reality, could vary within a deployment or between the sampling regions of PTV and DIH.

Looking to the future, we are determined to tackle these challenges head-on. A promising development in our arsenal is the introduction of the snow particle analyzer [27]. This tool offers direct measurements of snow particle properties, such as size, shape, type, and notably, density. By capturing these specifics in real-time field conditions, we pave the way for an intricate and precise quantification of snow particle aerodynamics. By employing models like the Best number [8], which is dependent on particle density, ambient air density and viscosity, particle diameter, and the projected area, we can now estimate snow terminal velocity. This estimation would allow for a more detailed calculation of the aerodynamic response time, reducing the need for broad assumptions and providing us with data from actual field conditions.

Moreover, the integration of 3D PTV technology is set to revolutionize our understanding of snow particle kinematics and the complex mechanics of snow particle clustering. This technology helps us visualize the settling trajectories and clustering patterns in three dimensions. It allows us to delve into the influence of particle morphology on their behavior, elucidating complex patterns like meandering and tumbling motions influenced by turbulence-induced instabilities [4,19,54]. Notably, the combination of 3D PTV and Voronoi analysis lends us the capability to visualize and quantify 3D snow clusters, leading to further insights into the behavior of snow particles within these clusters.

With the integration of our newly introduced snow particle analyzer and 3D PTV, we are well-positioned to extract more precise information about snow properties and dynamics in the field. This allows us to conduct systematic studies

under various turbulence and snow particle conditions. As a result, we can draw direct comparisons with well-controlled laboratory experiments, such as those conducted by [11,44,50], to elucidate the individual and combined effects of snow morphology and turbulence on snow settling.

The implications of these forthcoming investigations are considerable. Our efforts are likely to pave the way for the development of more robust and accurate models of snow settling dynamics. By establishing a comprehensive understanding of snow settling behaviors under realistic field conditions, we can create models that more accurately reflect the complexities of these processes. These improved models will not only serve as valuable tools for academic research but could also have practical applications in areas such as meteorology and climate science. By making predictions more precise, we can better anticipate, plan for, and respond to weather events and climate change impacts.

## References


1. Abraham, A., Hong, J.: Dynamic wake modulation induced by utility-scale wind turbine operation. Appl. Energy **257**, 114003 (2020)
2. Adrian, R., Christensen, K., Liu, Z.-C.: Analysis and interpretation of instantaneous turbulent velocity fields. Exp. Fluids **29**(3), 275–290 (2000)
3. Aliseda, A., Cartellier, A., Hainaux, F., Lasheras, J.C.: Effect of preferential concentration on the settling velocity of heavy particles in homogeneous isotropic turbulence. J. Fluid Mech. **468**, 77–105 (2002)
4. Auguste, F., Magnaudet, J., Fabre, D.: Falling styles of disks. J. Fluid Mech. **719**, 388–405 (2013)
5. Ayyalasomayajula, S., Gylfason, A., Collins, L.R., Bodenschatz, E., Warhaft, Z.: Lagrangian measurements of inertial particle accelerations in grid generated wind tunnel turbulence. Phys. Rev. Lett. **97**(14), 144507 (2006)
6. Balachandar, S., Eaton, J.K.: Turbulent dispersed multiphase flow. Annu. Rev. Fluid Mech. **42**, 111–133 (2010)
7. Bec, J., et al.: Acceleration statistics of heavy particles in turbulence. J. Fluid Mech. **550**, 349–358 (2006)
8. Böhm, H.P.: A general equation for the terminal fall speed of solid hydrometeors. J. Atmos. Sci. **46**(15), 2419–2427 (1989)
9. Bristow, N., Li, J., Hartford, P., Guala, M., Hong, J.: Imaging-based 3d particle tracking system for field characterization of particle dynamics in atmospheric flows. Exp. Fluids **64**(4), 1–14 (2023)
10. Dasari, T., Wu, Y., Liu, Y., Hong, J.: Near-wake behaviour of a utility-scale wind turbine. J. Fluid Mech. **859**, 204–246 (2019)
11. Esteban, L.B., Shrimpton, J., Ganapathisubramani, B.: Edge effects on the fluttering characteristics of freely falling planar particles. Phys. Rev. Fluids **3**(6), 064302 (2018)
12. Falkinhoff, F., Obligado, M., Bourgoin, M., Mininni, P.D.: Preferential concentration of free-falling heavy particles in turbulence. Phys. Rev. Lett. **125**(6), 064504 (2020)
13. Ferenc, J.-S., Néda, Z.: On the size distribution of poisson voronoi cells. Phys. A **385**(2), 518–526 (2007)

14. Ferrante, A., Elghobashi, S.: On the physical mechanisms of two-way coupling in particle-laden isotropic turbulence. Phys. Fluids **15**(2), 315–329 (2003)
15. Garrett, T.J., Bair, E.H., Fallgatter, C.J., Shkurko, K., Davis, R.E., Howlett, D.: The multi-angle snowflake camera. In: International Snow Science Workshop, pp. 16–21 (2012)
16. Garrett, T.J., Yuter, S.E.: Observed influence of riming, temperature, and turbulence on the fallspeed of solid precipitation. Geophys. Res. Lett. **41**(18), 6515–6522 (2014)
17. Good, G., Ireland, P., Bewley, G., Bodenschatz, E., Collins, L., Warhaft, Z.: Settling regimes of inertial particles in isotropic turbulence. J. Fluid Mech. **759**, R3 (2014)
18. Heisel, M., Dasari, T., Liu, Y., Hong, J., Coletti, F., Guala, M.: The spatial structure of the logarithmic region in very-high-reynolds-number rough wall turbulent boundary layers. J. Fluid Mech. **857**, 704–747 (2018)
19. Herzhaft, B., Guazzelli, É.: Experimental study of the sedimentation of dilute and semi-dilute suspensions of fibres. J. Fluid Mech. **384**, 133–158 (1999)
20. Heymsfield, A.J., Westbrook, C.: Advances in the estimation of ice particle fall speeds using laboratory and field measurements. J. Atmos. Sci. **67**(8), 2469–2482 (2010)
21. Hong, J., et al.: Natural snowfall reveals large-scale flow structures in the wake of a 2.5-mw wind turbine. Nat. Commun. **5**(1), 4216 (2014)
22. Ireland, P.J., Bragg, A.D., Collins, L.R.: The effect of Reynolds number on inertial particle dynamics in isotropic turbulence. Part 2. Simulations with gravitational effects. J. Fluid Mech. **796**, 659–711 (2016)
23. Ishihara, T., Kaneda, Y., Yokokawa, M., Itakura, K., Uno, A.: Small-scale statistics in high-resolution direct numerical simulation of turbulence: Reynolds number dependence of one-point velocity gradient statistics. J. Fluid Mech. **592**, 335–366 (2007)
24. Khvorostyanov, V.I., Curry, J.A.: Terminal velocities of droplets and crystals: power laws with continuous parameters over the size spectrum. J. Atmos. Sci. **59**(11), 1872–1884 (2002)
25. Li, C., et al.: Settling and clustering of snow particles in atmospheric turbulence. J. Fluid Mech. **912**, A49 (2021)
26. Li, J., Abraham, A., Guala, M., Hong, J.: Evidence of preferential sweeping during snow settling in atmospheric turbulence. J. Fluid Mech. **928**, A8 (2021)
27. Li, J., Guala, M., Hong, J.: Snow particle analyzer for simultaneous measurements of snow density and morphology. J. Geophys. Res.: Atmos. **128**(16), e2023JD038987 (2023). https://doi.org/10.1029/2023JD038987
28. Locatelli, J.D., Hobbs, P.V.: Fall speeds and masses of solid precipitation particles. J. Geophys. Res. **79**(15), 2185–2197 (1974)
29. Magono, C., Lee, C.W.: Meteorological classification of natural snow crystals. J. Faculty Sci. Hokkaido Univ. Ser. 7, Geophys. 2 **4** , 321–335 (1966)
30. Mallery, K., Shao, S., Hong, J.: Dense particle tracking using a learned predictive model. Exp. Fluids **61**(10), 1–14 (2020). https://doi.org/10.1007/s00348-020-03061-y
31. Marks, D., Kimball, J., Tingey, D., Link, T.: The sensitivity of snowmelt processes to climate conditions and forest cover during rain-on-snow: a case study of the 1996 pacific northwest flood. Hydrol. Process. **12**(10–11), 1569–1587 (1998)
32. Maxey, M.R., Riley, J.J.: Equation of motion for a small rigid sphere in a nonuniform flow. Phys. Fluids **26**(4), 883–889 (1983)

33. Mitchell, D.L., Heymsfield, A.J.: Refinements in the treatment of ice particle terminal velocities, highlighting aggregates. J. Atmos. Sci. **62**(5), 1637–1644 (2005)
34. Mitchell, D.L., Zhang, R., Pitter, R.L.: Mass-dimensional relationships for ice particles and the influence of riming on snowfall rates. J. Appl. Meteorol. Climatol. **29**(2), 153–163 (1990)
35. Mordant, N., Crawford, A.M., Bodenschatz, E.: Experimental lagrangian acceleration probability density function measurement. Physica D **193**(1–4), 245–251 (2004)
36. Nemes, A., Dasari, T., Hong, J., Guala, M., Coletti, F.: Snowflakes in the atmospheric surface layer: observation of particle-turbulence dynamics. J. Fluid Mech. **814**, 592–613 (2017)
37. Ogura, T., Kageyama, I., Nasukawa, K., Miyashita, Y., Kitagawa, H., Imada, Y.: Study on a road surface sensing system for snow and ice road. JSAE Rev. **23**(3), 333–339 (2002)
38. Ouellette, N.T., Xu, H., Bodenschatz, E.: A quantitative study of three-dimensional lagrangian particle tracking algorithms. Exp. Fluids **40**, 301–313 (2006)
39. Passarelli, Jr., R.E.: Theoretical and observational study of snow-size spectra and snowflake aggregation efficiencies. J. Atmos. Sci. **35**(5), 882–889 (1978)
40. Petersen, A.J., Baker, L., Coletti, F.: Experimental study of inertial particles clustering and settling in homogeneous turbulence. J. Fluid Mech. **864**, 925–970 (2019)
41. Raffel, M., Willert, C.E., Scarano, F., Kähler, C.J., Wereley, S.T., Kompenhans, J.: Particle Image Velocimetry. Springer, Cham (2018). https://doi.org/10.1007/978-3-319-68852-7
42. Rosa, B., Parishani, H., Ayala, O., Wang, L.-P.: Settling velocity of small inertial particles in homogeneous isotropic turbulence from high-resolution dns. Int. J. Multiph. Flow **83**, 217–231 (2016)
43. Shaw, R.A.: Particle-turbulence interactions in atmospheric clouds. Annu. Rev. Fluid Mech. **35**(1), 183–227 (2003)
44. Siewert, C., Kunnen, R., Meinke, M., Schröder, W.: Orientation statistics and settling velocity of ellipsoids in decaying turbulence. Atmos. Res. **142**, 45–56 (2014)
45. Steinkogler, W., Sovilla, B., Lehning, M.: Influence of snow cover properties on avalanche dynamics. Cold Reg. Sci. Technol. **97**, 121–131 (2014)
46. Tagliavini, G., Khan, M.H., McCorquodale, M., Westbrook, C., Holzner, M.: Wake characteristics of complex-shaped snow particles: Comparison of numerical simulations with fixed snowflakes to time-resolved particle tracking velocimetry experiments with free-falling analogs. Phys. Fluids **34**(5), 055112 (2022)
47. Tagliavini, G., McCorquodale, M., Westbrook, C., Corso, P., Krol, Q., Holzner, M.: Drag coefficient prediction of complex-shaped snow particles falling in air beyond the stokes regime. Int. J. Multiph. Flow **140**, 103652 (2021)
48. Tan, S., Salibindla, A., Masuk, A.U.M., Ni, R.: Introducing openlpt: new method of removing ghost particles and high-concentration particle shadow tracking. Exp. Fluids **61**, 1–16 (2020)
49. Theriault, D.H., et al.: A protocol and calibration method for accurate multi-camera field videography. J. Exp. Biol. **217**(11), 1843–1848 (2014)
50. Tinklenberg, A., Guala, M., Coletti, F.: Thin disks falling in air. J. Fluid Mech. **962**, A3 (2023)
51. Toloui, M., et al.: Measurement of atmospheric boundary layer based on super-large-scale particle image velocimetry using natural snowfall. Exp. Fluids **55**(5), 1–14 (2014). https://doi.org/10.1007/s00348-014-1737-1
52. Tom, J., Bragg, A.D.: Multiscale preferential sweeping of particles settling in turbulence. J. Fluid Mech. **871**, 244–270 (2019)

53. Voth, G.A., La Porta, A., Crawford, A.M., Alexander, J., Bodenschatz, E.: Measurement of particle accelerations in fully developed turbulence. J. Fluid Mech. **469**, 121–160 (2002)
54. Voth, G.A., Soldati, A.: Anisotropic particles in turbulence. Annu. Rev. Fluid Mech. **49**, 249–276 (2017)
55. Wang, L.-P., Maxey, M.R.: Settling velocity and concentration distribution of heavy particles in homogeneous isotropic turbulence. J. Fluid Mech. **256**, 27–68 (1993)
56. Yang, C., Lei, U.: The role of the turbulent scales in the settling velocity of heavy particles in homogeneous isotropic turbulence. J. Fluid Mech. **371**, 179–205 (1998)
57. Zhou, J., Adrian, R.J., Balachandar, S., Kendall, T.: Mechanisms for generating coherent packets of hairpin vortices in channel flow. J. Fluid Mech. **387**, 353–396 (1999)